

BA PB 429/1



Pergamon

Geochimica et Cosmochimica Acta, Vol. 62, No. 16, pp. 2739-2756, 1998
Copyright © 1998 Elsevier Science Ltd
Printed in the USA. All rights reserved
0016-7037/98 \$19.00 + .00

PII S0016-7037(98)00185-9

ISSN

⁴⁰Ar/³⁹Ar dating of West African lateritic cryptomelanes

O. HÉNOUCQUE,^{*1} G. RUFFET,² F. COLIN,^{1,3} G. FÉRAUD²

¹UMR CNRS 6635, CEREGE, BP 80, 13545 Aix-en-Provence Cedex 4, France

²Géosciences Azur, UMR CNRS 6526, UNSA, Parc Valrose, 06108 Nice Cedex 2, France

³ORSTOM, 213 rue Lafayette, 75480 Paris Cedex, France

(Received May 27, 1997; accepted in revised form May 11, 1998)

Abstract—Dating weathering processes is an innovative approach to understanding climate-dependant modifications of the Earth's surface. Potassium-bearing manganese oxides are a ubiquitous feature of weathering mantles developed from Mn-bearing parent rocks. Recent studies have demonstrated the possibility of dating K-rich manganese oxides from the hollandite group, such as cryptomelane (K₁₋₂Mn₈O₁₆·nH₂O), using ⁴⁰Ar/³⁹Ar argon-ion laser probe method. This work applies that approach to cryptomelanes formed in the lateritic manganese ore deposit of Tambao (northern Burkina Faso), a present unexploited deposit among the cryptomelane-richest in the world. Two samples of massive Mn-rich concretions (10mm and 4mm in thickness) were collected from the massive 80-m high Mn-rich hill at Tambao. A detailed petrographical study shows that these cortical formations are composed of successive Na-rich cryptomelane layers, with Na/(Na + K + Ba) up to 20%. Seven and five subsamples from these two concretions were studied with a ⁴⁰Ar/³⁹Ar laser probe. The age spectra indicate ages that are coherent with the general organization of the concretions, showing a regular decrease from cores towards rims. Within the two concretions, ages range from 49.8 ± 0.4 Ma to 48.1 ± 0.1 Ma, and from 47.5 ± 0.3 Ma to 44.5 ± 0.4 Ma, respectively, the youngest ages being obtained for the most external layers. The integrated rates of cryptomelane precipitation are estimated at 1 and 5 mm/Ma. These ages clusters show that weathering at Tambao was functioning during the early Eocene and thus suggest that there is a relationship between the formation of the bauxites of the African Surface and the Mn-Fe laterites. Copyright © 1998 Elsevier Science Ltd

INTRODUCTION

Chemical and mechanical weathering-derived processes are among the most efficient factors in modifying the Earth surface. Over geological times, weathering gradients are dependent on temperature, rainfall, and tectonic stability. In this way, the surficial domains of the present day tropical and subtropical cratons have been transformed since the early Tertiary into thick supergene lateritic sequences often associated with metal accumulation. Such massive indurated crusts, which are frequently resistant to erosion (Boulangé, 1984; Nahon, 1986; Nahon et al., 1985, 1991; Beauvais and Colin, 1993), could constitute a long-time record of past climate evolution.

Direct dating of weathering events was difficult until the development of microbeam methods. One of the most promising approaches is ⁴⁰Ar/³⁹Ar dating of isotopically closed supergene K-bearing minerals from the hollandite group (α-MnO₂). Minerals from this group have a tunnel structure, constituted of double chains of MnO₆ octahedra combined at corners, and denoted T(2,2) in the nomenclature proposed by Turner and Buseck (1981). The generic chemical formula of minerals from the hollandite group is A_xB₈O₁₆·nH₂O. The large cations, such as K⁺, Ba²⁺, Pb²⁺, Na⁺, occupy A sites and maintain the charge balance. The mineral name reflects the cations occupying A sites. K⁺ corresponds to cryptomelane, Ba²⁺ to hollandite, Pb²⁺ to coronadite and Na⁺ to manjiroite. All of these minerals generally occur as solid solutions in natural environment. The term cryptomelane, used in our paper,

defines minerals in which K⁺ is the main cation, even if other cations are present. B sites, which are formed by the cation-oxygen octhedra, contain Mn⁴⁺, Mn³⁺, Fe³⁺ and so on (Byström and Byström, 1950; Wadsley, 1953; Turner and Buseck, 1979; McKenzie, 1989).

In the 60s, Chukhrov et al. (1966) performed the first K-Ar dating of potassium-rich manganese oxides, described as "fine mixtures of cryptomelane with other hypergenous manganese minerals." Their "psilomelane" samples, from Kazakhstan and Kerch Peninsula deposits, had developed from alteration of braunite, hausmannite, and manganese siderite.

Yashvili and Gukasyan (1974) first succeeded in studying monomineral fractions of K-Ba manganese oxides of hydrothermal origin, from the Sevkar-Sargyukh manganese deposit (Armenia). Their K-Ar results proved the capacity for cryptomelane to retain radiogenic argon.

Recent development of the ⁴⁰Ar/³⁹Ar laser probe method stimulated renewed interest in such studies (Vasconcelos et al., 1992, 1994; Ruffet et al., 1996). The very low amount of material necessary for analysis with this new approach allows a fine scale sampling, making it possible to date distinct generations of K-Mn oxides.

Vasconcelos et al. (1992, 1994) applied step-heating argon-ion laser ⁴⁰Ar/³⁹Ar mass spectrometry to study several manganese weathering profiles from Brazil, demonstrating that direct dating of weathering phenomena was possible. Their work confirmed that cryptomelane is a suitable mineral for dating, even if problems related to contamination by hypogene phases or presence of multiple generations of manganese oxide were encountered.

Cryptomelane is present in numerous lateritic manganese

*Author to whom correspondence should be addressed (henocque@cerege.fr).



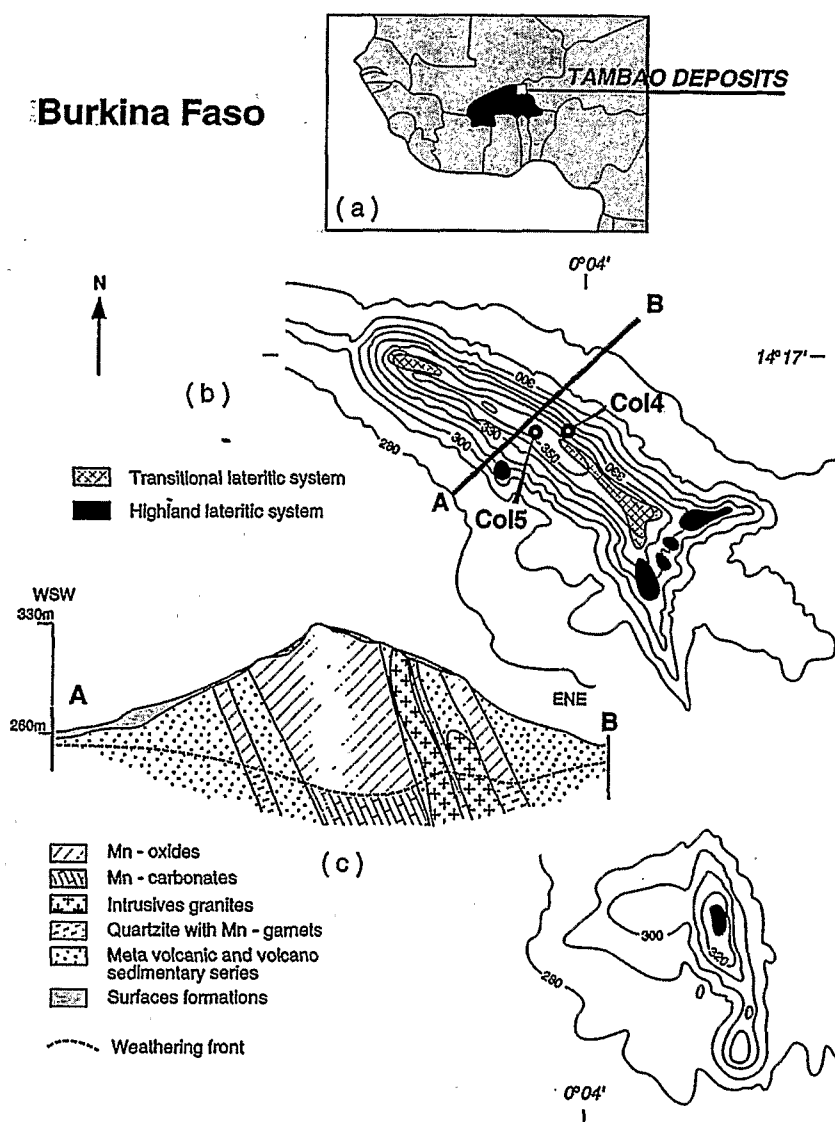


Fig. 1. (a) Location of the Tambaio Manganese deposit. (b) Topographical map of the Mn-rich formations and samples location. (c) Sketch of the main geological formations.

weathering profiles in South America, Africa, and Australia (Holtrop, 1965; Grandin, 1976; Nahon et al., 1984.; Perseil and Grandin, 1985). We propose to expand the scope of previous studies (Vasconcelos et al., 1992; Ruffet et al., 1996) to enhance our understanding of the genesis of Mn-lateritic systems (and potentially of Fe-laterites) throughout the tropical belt.

This work presents the analytical performances of the $^{40}\text{Ar}/^{39}\text{Ar}$ argon-ion laser probe method in dating successive cryptomelane generations in concretions collected at Tambaio deposit (Burkina Faso), one of the cryptomelane-richest deposit known in the world (Grandin, 1976). These $^{40}\text{Ar}/^{39}\text{Ar}$ results are the first measured ages from a lateritic sequence from Africa.

2. GEOGRAPHICAL, GEOLOGICAL, AND SAMPLE SETTING

The manganese ore deposit of Tambaio is located in the northern part of Burkina Faso (14°17'N, 0°4'E), in the sub-

sahelian area (Fig. 1). Composed of two hills, it constitutes a reserve of about 15 Mt of a manganese-rich ore with a manganese oxide content greater than 50%. The manganese oxide layers alternate with quartzite and schist, within the weathered Birimian metavolcanic and volcano-sedimentary series. In the main hill, about 70% of the manganese oxides result from in situ weathering of a rhodochrosite bed observed in drilling cores (Picot and Trinquard, 1969). The rest is derived from a silicified metamorphic protore with Mn-rich garnets (spessartite) described by Grandin (1976) and Perseil and Grandin (1978, 1985). Metamorphism of these formations is associated with granitic intrusions, which are also affected by weathering. Kaolinite is ubiquitous in the whole deposit, even within the manganese oxide benches that preserve some of the primary structures (folds) and schistosity of the parent rocks. Oxidation of the manganese carbonate protore is accompanied by a significant volume loss that is the origin of numerous dissolutional structures, such as karstic voids, observed in the whole

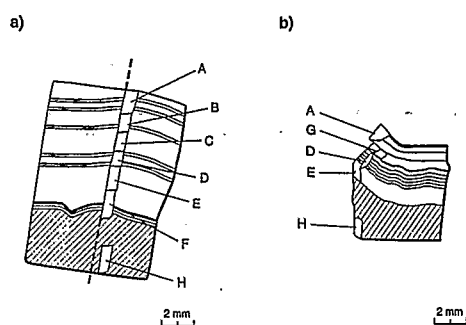


Fig. 2. Sketch of the studied 500 μm thick rock slabs showing the two cortices organization and the relative positions of the extracted submillimetric samples. (a) Col 4 and (b) Col 5.

manganese deposit. Supergene manganese-rich concretions and stalactites have developed within such voids.

In Africa, successive lateritic episodes with specific types of more or less indurated crusts characterize various stages of regional morphogenesis (Nahon, 1991; Beauvais and Colin, 1993). Bauxites, usually attributed to the Cretaceous-Eocene period, are located in the highest topographical positions. The lowest reliefs correspond to younger quartzo-ferruginous systems, presumably formed since the Miocene and throughout the Pliocene and Quaternary (Brown et al., 1994; Colin et al., 1997). Between Bauxites and the quartzo-ferruginous systems, an either ferruginous or manganiferous lateritic system has been described in many African countries (Grandin, 1976; Boulangé, 1983; Sanfo, 1994). Such a system is called transitional lateritic system by Grandin (1976). The highest Fe-Mn pisolitic crust of the largest hill of the Tambao deposit is considered to be a relict of this transitional lateritic system (Grandin, 1976).

The present study examines two concretions collected on the main hill. The first one (Col4) was sampled in a trench cross-cutting the northeastern slope of the hill at about 20 m below the summit. It presents a botryoidal aspect with a cortex composed of regular concentric gray bands that develop over 1 cm around an inhomogeneous blackish core. The second sample (Col5) was collected on the crest of the hill within a formation preserving the primary schistosity of the carbonated protore. This sample presents an heterogeneous aspect consisting of thin gray concretions, with a total thickness of 4 mm, that separate two black massive granular bands (Fig. 2).

3. MINERALOGY AND PETROGRAPHY

Cryptomelanes were studied by X-ray diffraction, using a Philips PW 1710 diffractometer with a Co-tube anode ($\kappa\alpha_1 = 1.78896$; $\kappa\alpha_2 = 1.79285$). The cell parameters were calculated with an indexing and least square powder diffraction program. The chemical compositions of the successive cryptomelane generations were determined through eighty microprobe analyses, using a CAMEBAX microprobe set (15 kV, 20 mA, 1 μm size diameter).

The x-ray diffraction analyses performed on whole rock powders show that cryptomelane is the main mineralogical phase. Comparison of observed diffraction peaks and calculated cell parameters with the ASTM-parameters indicates that

Table 1. Comparison between cryptomelane ASTM (20.908) and calculated parameters.

Cryptomelane ASTM 20.908		Col 4	Col 5
hkl	d (Å)	d (Å)	d (Å)
110	6.900	6.906	6.929
200	4.900	4.911	4.945
310	3.100	3.112	2.3114
400, 201	2.460	2.462	2.467
410, 211	2.390	2.395	2.396
420, 221	2.190	2.199	
301	2.150	2.150	2.152
520, 411	1.830	1.830	1.831
600	1.640	1.643	
521	1.540	1.540	1.542
002, 601	1.420	1.425	1.424
Tetragonal			
a = b	9.84	9.851	9.866
c	2.85	2.848	2.848
v	275.48	276.4	277.22

cryptomelane in the cortices from samples Col4 and Col5 is well crystallized (Table 1). Some analyses, however, indicate the presence of lithiophorite in the outer part of the cortex of sample Col4. Na-rich cryptomelane is detected in both cortices by long time diffraction directly on rock slabs (Fig. 3a and 3b). Its presence is indicated by a displacement of the diffraction peaks corresponding to a weak modification of the d-values in the crystal structure. The proportions of this Na-pole have been determined using the electron microprobe data. The x-ray analyses performed on the core of the concretions revealed the presence of nsutite and lithiophorite.

Reflected light microscopy examinations show that the central parts of our samples are composed of other manganese oxides that could not be identified by x-ray diffraction analysis. In this way, hausmannite, with its characteristic twinned appearance, was clearly identified in sample Col4. This mineral is partly transformed into a cryptomelane-rich matrix with minor nsutite and small ramsdellite domains. Pyrolusite is also observed in sample Col5. The cryptomelane matrix develops generally between hausmannite domains and internal rims of the cortices (Fig. 4). In the central part of the samples, macropores are preferential sites for concentric crystallization of cryptomelane and lithiophorite.

The cortices show a succession of optically distinct layers. The reflectance of these layers is moderate and seems to vary with the overall appearance of the oxide crystals. Sometimes cryptocrystalline in the thinnest layers, cryptomelane is generally well crystallized with a needle shape, in the thickest ones. The outermost layer of Col4 cortex is composed of a pure and very well crystallized lithiophorite, with 100 μm long fibroradial crystals (Fig. 5). A similar layer is observed in sample Col5, with a thickness that does not exceed a few μm . The cortex of this concretion is covered by an irregular goethitic and clayey cement that contains small quartz grains.

Electron microprobe analyses were performed on successive layers of the two concretions. These measurements show that the composition does not significantly vary within single layers and that there is no regular evolution between the inner and outer parts of the cortices, especially for sample Col4, despite

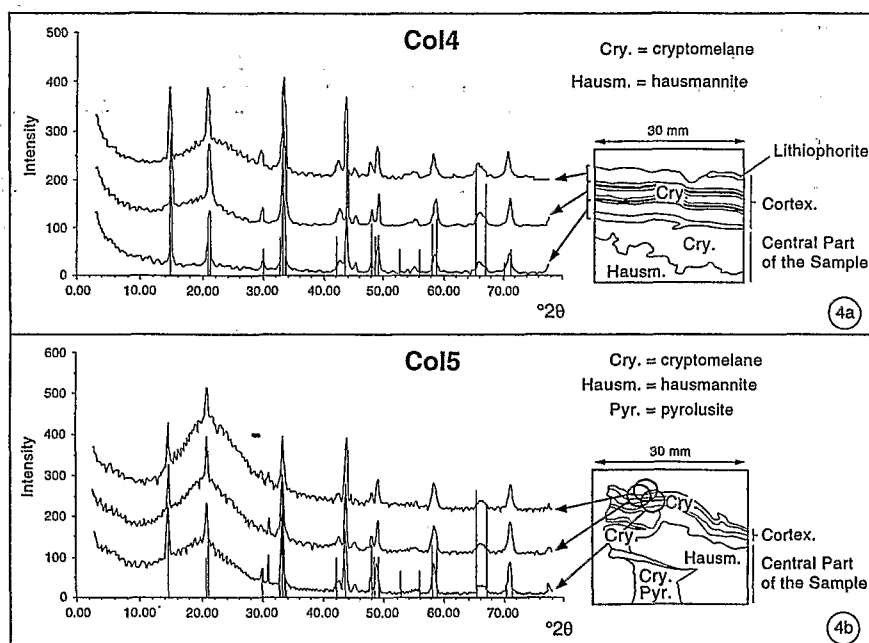


Fig. 3. X-ray diffraction diagrams of samples Col 4 and Col 5 compared to the standard diffraction peaks of cryptomelane (ASTM 20.908) and sketch of the thin section showing the spatial relationships of the studied phases. (a) X-ray diffraction diagram obtained from sample Col 4 rock slab. (b) X-ray diffraction diagram obtained from sample Col 5 rock slab.

strong variations of the K_2O content (3.5–6.2%). Variations are not so extensive in sample Col5, with K_2O contents ranging from 4.9% to 5.7% (Tables 2 and 3). The results of the two profiles are plotted along sketches of the two polished sections (Fig. 6). The chemical elements displayed characterize either cryptomelane (K), hollandite (Ba) or manjiroite (Na) poles. Aluminum contents may indicate the presence of clay minerals or lithiophorite, but Al may also substitute for Mn as observed for the hollandite group minerals (Byström and Byström, 1950).

The low amounts of Ba show that cryptomelane and manjiroite (K and Na endmembers of the hollandite group) are the dominant constituents of the solid solution. The high Al content (about 10% of Al_2O_3) in the outer part of the cortex of sample Col5 are due primarily to the clayey-goethitic matrix and secondarily to the outermost lithiophorite-cryptomelane layer of the cortex. It should be noted that the Na-profile of sample Col4 shows a clear disturbance at 8mm that correlates with variations observed in the other elements. These chemical changes, which are centered on a group of small layers optically observed, confirm that the optical limits between layers are also geochemical discontinuities.

These different methods of investigations show that cryptomelane is the main mineral phase of the cortices. The optical observations and microprobe measurements suggest that each layer of the cortices is a mineralogical system that is distinct from adjacent layers and that corresponds to the growth of a new generation of oxides. Each layer or oxide generation could result from different percolating solutions within the weathering profile.

The organization of the central parts of the concretions, out of the cortices, is more complex. It probably results from two distinct phenomena:

- secondary in situ crystallization with replacement of Mn^{2+} and Mn^{3+} phases (hausmannite and manganosite) by more oxidized (Mn^{3+} and Mn^{4+}) manganiferous phases (cryptomelane, ramsdellite, nsutite, and pyrolusite);
- concentric crystallization in macroporosity of Mn^{3+} and Mn^{4+} oxides (cryptomelane and lithiophorite).

4. $^{40}Ar/^{39}Ar$ ANALYTICAL PROCEDURE

Seven and five submillimetric fragments were extracted from thin slabs (0.5 mm thick) cut perpendicularly to the growth direction of the concretions Col4 and Col5. The relative positions of the extracted fragments within the cortices and inner parts of the concretions are presented in Fig. 2. The samples were wrapped in Al-foil. The Al-packets were stacked to form a column within which packets of flux monitors were inserted every eight to ten samples. This distribution allows precise determination of the vertical flux gradient during irradiation and yields $^{40}Ar/^{39}Ar_K$ ratios of the monitors with errors as low as $\pm 0.2\%$. The samples were irradiated in the 5C position of the McMaster reactor (Hamilton, Canada); four samples (Col4-c, e, f, and h) were irradiated for 5 hours (irradiation MC7) together with biotite monitor Bern4B (17.25 Ma; Hall et al., 1984) and ten samples (Col4-a, b, c, d, e and Col5-a, g, d, e, and h) for 70 hours (irradiation MC8) together with amphibole monitor Zartman Hb3gr (Zartman, 1964; Turner, 1971; Roddick, 1983; 1072 Ma).

Step heating experiments on single grains, described in detail by Ruffet et al. (1991), were performed with a laser-probe using a Coherent Innova 70-4 continuous argon-ion laser with a maximum output power of 6 W in multiline mode. The laser beam was defocused through an optical system onto a sample located in a UHV sample chamber (a copper sample-holder,

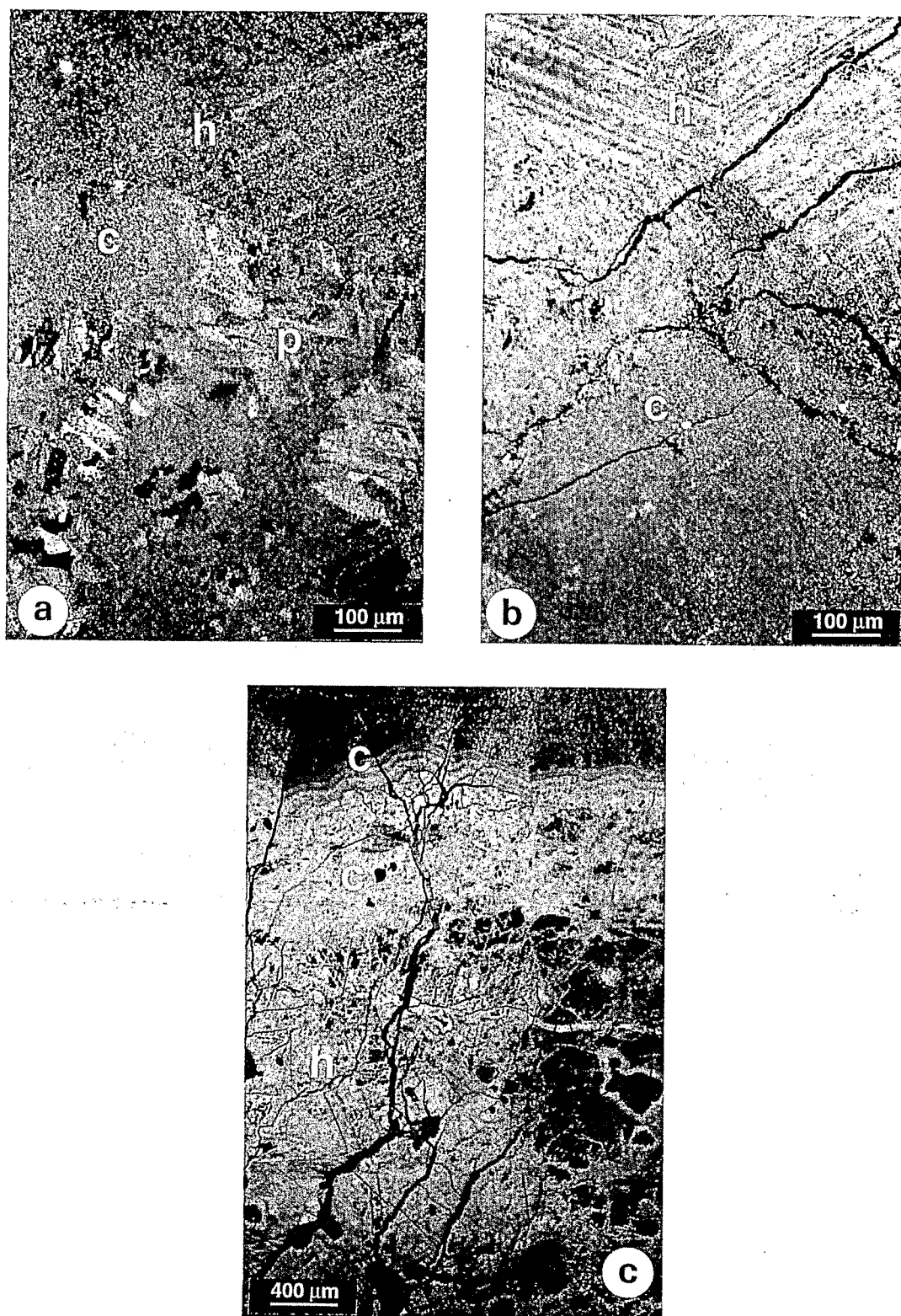


Fig. 4. (a) Microphotograph showing the transition between hausmannite and cryptomelane matrix with few ramsdellite in sample Col4 core. $\times 160$ under polarized light. (b) Microphotograph showing the transition between hausmannite and cryptomelane-pyrolusite matrix in sample Col5 core. $\times 160$ under polarized light. (c) Microphotograph of sample Col 4 showing the cryptomelane matrix developed between the hausmannite domain and the first layer of the cortex. $\times 40$ under polarized light.

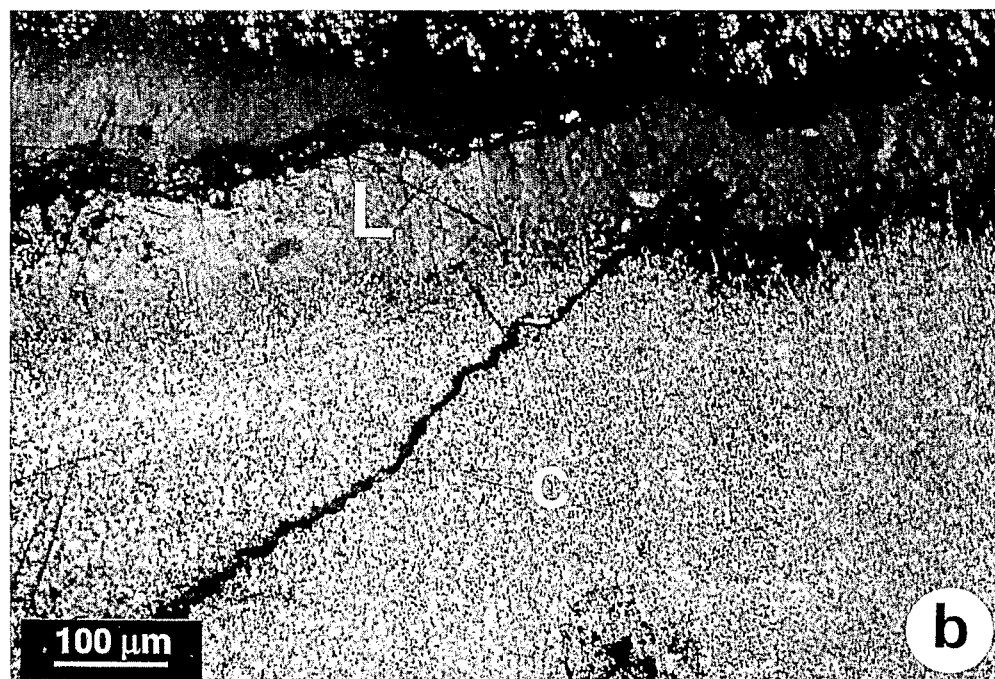
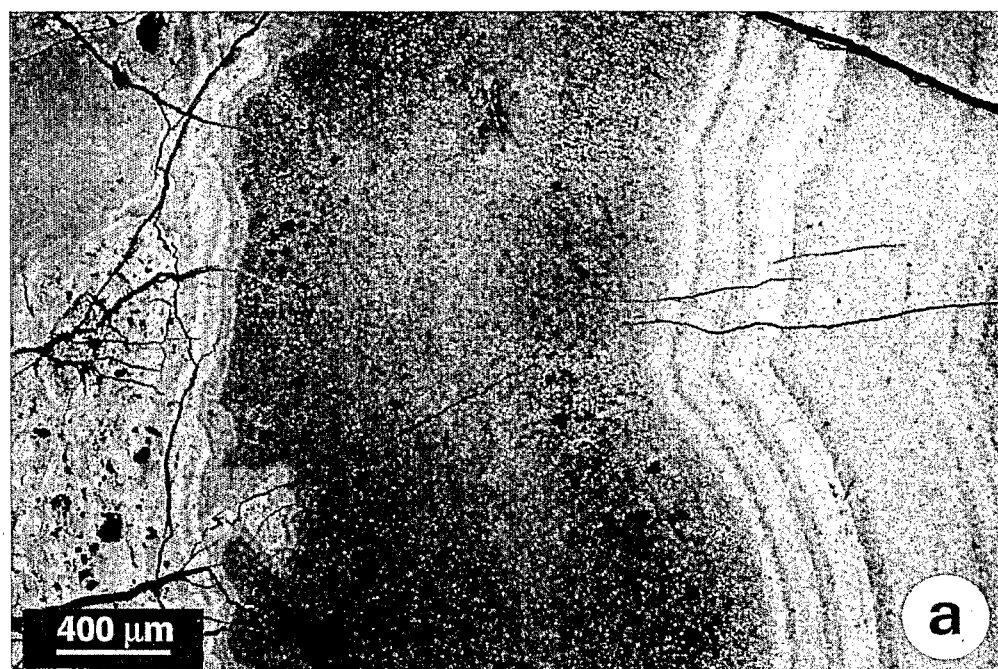


Fig. 5. (a) Microphotograph of sample Col 4. The reflectance of the successive layers depends on the global crystallinity of cryptomelane (density and dimension) $\times 40$. (b) Microphotograph of the external rim of sample Col 4 which is composed of a pure lithiophorite layer developed over $100 \mu\text{m}$. $\times 160$ under polarized light.

beneath a Pyrex window, in a stainless steel chamber). Each laser experiment lasted 3 min, including 1 min for the laser heating of the sample. The laser beam was at least 2.5 times greater than the sample size, in order to obtain a homogeneous

temperature over the whole grain. The temperature is not known but its homogeneity was assessed by observing the heated mineral with a binocular microscope coupled with a video color camera and a high-resolution video recorder. The

Table 2. Electron microprobe data for sample Col 4 and calculated cryptomelane formulas. Formulas based on 16 O atoms. (in) and (out) indicates respectively the intern and extern parts of the cortical formation; positions reflect precisely microprobe coordinates.

	Positions (mm)																			(out)
	(in)	9.8	9.5	9	8.55	8.5	8.45	8.4	8.3	8.2	8	7.5	7	6	5	4	3	1.5	1	
SiO ₂	0.326	0.463	0.457	0.337	0.339	0.477	0.425	0.324	0.433	0.317	0.513	0.569	0.438	0.526	0.402	0.361	0.421	0.379	0.476	SiO ₂
Al ₂ O ₃	0.383	0.466	0.301	0.270	0.269	0.258	0.156	0.210	0.182	0.334	0.551	0.598	0.728	0.569	0.401	0.507	0.229	0.184	0.300	Al ₂ O ₃
Fe ₂ O ₃	0.110	0.063	0.119	0.190	0.044	0.071	0.057	0.095	0.099		0.048	0.092	0.046	0.115	0.079	0.044	0.131	0.084	0.090	Fe ₂ O ₃
MnO ₂	85.494	85.019	85.115	86.285	86.134	86.358	86.458	87.114	86.639	86.790	85.241	83.309	85.420	85.217	84.524	85.831	86.890	85.879	83.535	MnO ₂
MgO											0.028									MgO
CaO	0.207	0.100	0.057	0.112	0.066	0.127	0.122	0.114	0.065	0.097	0.135	0.045	0.039	0.079	0.058	0.076	0.093	0.070	0.054	CaO
Na ₂ O	0.919	0.272	0.282	0.590	0.574	0.468	0.311	0.740	0.325	0.274	0.253	0.277	0.177	0.153	0.213	0.245	0.260	0.230	0.187	Na ₂ O
K ₂ O	4.737	6.153	5.363	4.479	4.939	4.292	5.887	4.647	5.852	4.971	4.717	6.144	5.919	5.188	5.891	5.140	3.472	3.505	4.261	K ₂ O
TiO ₂																				TiO ₂
Cr ₂ O ₃																				Cr ₂ O ₃
NiO	0.089	0.049	0.013	0.029	0.039	0.058		0.053		0.021	0.028	0.015		0.019						NiO
BaO	0.048	0.015					0.024	0.024					0.026	0.056	0.059	0.047	0.035	0.107	0.071	BaO
Total	92.31	92.6	91.707	92.292	92.404	92.109	93.44	93.321	93.595	92.804	91.514	91.049	92.793	91.922	91.627	92.251	91.531	90.438	88.974	Total
Si	0.04	0.06	0.06	0.04	0.05	0.06	0.05	0.04	0.06	0.04	0.07	0.08	0.06	0.07	0.05	0.05	0.05	0.05	0.06	Si
Al	0.06	0.07	0.05	0.04	0.04	0.04	0.02	0.03	0.03	0.05	0.08	0.09	0.11	0.09	0.06	0.08	0.03	0.03	0.05	Al
Fe	0.01	0.01	0.01	0.02		0.01	0.01	0.01	0.01		0.01	0.01		0.01	0.01		0.01	0.01	0.01	Fe _{3t}
Mn	7.63	7.6	7.65	7.68	7.67	7.69	7.65	7.68	7.65	7.69	7.64	7.57	7.60	7.62	7.63	7.66	7.74	7.75	7.69	Mn
Mg											0.01									Mg
Ca	0.03	0.01	0.01	0.02	0.01	0.02	0.02	0.02	0.01	0.01	0.02	0.01	0.01	0.01	0.01	0.01	0.01	0.01	0.01	Ca
Na	0.23	0.07	0.07	0.15	0.14	0.12	0.08	0.18	0.08	0.07	0.06	0.07	0.04	0.04	0.05	0.06	0.07	0.06	0.05	Na
K	0.78	1.02	0.89	0.74	0.81	0.71	0.97	0.76	0.96	0.82	0.78	1.03	0.98	0.86	0.98	0.85	0.57	0.59	0.73	K
Ti																				Ti
Cr																				Cr
Ni	0.01	0.01				0.01		0.01												Ni
Ba																		0.01		Ba
Total	8.79	8.85	8.74	8.69	8.72	8.66	8.8	8.73	8.80	8.68	8.67	8.86	8.80	8.70	8.79	8.71	8.48	8.51	8.60	Total
A	1.04	1.10	0.97	0.91	0.96	0.85	1.07	0.96	1.05	0.90	0.87	1.11	1.03	0.91	1.04	0.92	0.65	0.67	0.79	A
B	7.75	7.75	7.77	7.78	7.76	7.81	7.73	7.77	7.75	7.78	7.80	7.75	7.77	7.79	7.75	7.79	7.83	7.84	7.81	B
K pole	0.75	0.93	0.92	0.81	0.84	0.84	0.91	0.79	0.91	0.91	0.90	0.93	0.95	0.95	0.94	0.92	0.88	0.88	0.92	K pole
Na pole	0.22	0.06	0.07	0.16	0.15	0.14	0.07	0.19	0.08	0.08	0.07	0.06	0.04	0.04	0.05	0.07	0.11	0.09	0.06	Na pole
Ba pole	0.00	0.00	0.00	0.00	0.00	0.00	0.00	0.00	0.00	0.00	0.00	0.00	0.00	0.00	0.00	0.00	0.00	0.01	0.00	Ba pole

Table 3. Electron microprobe data for sample Col 5 and calculated cryptomelane formulas. Formulas based on 16 O atoms. (in) and (out) indicates respectively the intern and extern parts of the cortical formation; positions reflect precisely microprobe coordinates.

	Positions (mm)									(out)
	(in)	4.0	3.5	3.0	2.5	2.0	1.5	1.0	0.5	
SiO ₂	0.592	0.467	0.473	0.453	0.536	0.551	0.520	0.577	11.214	SiO ₂
Al ₂ O ₃	0.472	0.415	0.538	0.496	0.334	0.568	0.892	0.842	9.378	Al ₂ O ₃
Fe ₂ O ₃	0.251	0.047	0.054	0.124	0.080	0.155	0.087	0.159	4.355	Fe ₂ O ₃
MnO ₂	84.630	84.270	83.955	84.528	86.897	87.361	84.904	85.271	40.342	MnO ₂
MgO				0.023					0.047	MgO
CaO	0.077	0.090	0.002	0.027	0.184	0.025	0.033	0.057	0.135	CaO
Na ₂ O	0.233	0.157	0.460	0.539	0.432	0.115	0.331	0.190	0.079	Na ₂ O
K ₂ O	5.715	5.417	5.452	5.420	4.941	5.443	5.425	5.458	2.393	K ₂ O
TiO ₂									0.146	TiO ₂
Cr ₂ O ₃							0.014	0.027		Cr ₂ O ₃
NiO	0.030		0.017		0.022	0.015	0.046		0.028	NiO
BaO		0.044				0.020	0.008	0.171	0.174	BaO
Total	92.000	90.907	90.951	91.610	93.426	94.253	92.260	92.752	68.291	Total
Si	0.08	0.06	0.06	0.06	0.07	0.07	0.07	0.07		Si
Al	0.07	0.06	0.08	0.08	0.05	0.08	0.14	0.13		Al
Fe	0.03	0.01	0.01	0.01	0.01	0.02	0.01	0.02		Fe _{3t}
Mn	7.59	7.64	7.61	7.61	7.65	7.62	7.57	7.57		Mn
Mg										Mg
Ca	0.01	0.01			0.03			0.01		Ca
Na	0.06	0.04	0.12	0.14	0.11	0.03	0.08	0.05		Na
K	0.95	0.91	0.92	0.90	0.81	0.88	0.90	0.90		K
Ti										Ti
Cr										Cr
Ni										Ni
Ba								0.01		Ba
Total	8.79	8.73	8.80	8.80	8.73	8.70	8.77	8.76		Total
A	1.02	0.96	1.04	1.04	0.95	0.91	0.98	0.97		A
B	7.77	7.77	7.76	7.76	7.78	7.79	7.79	7.79		B
K pole	0.93	0.95	0.88	0.87	0.85	0.97	0.92	0.93		K pole
Na pole	0.06	0.04	0.12	0.13	0.12	0.03	0.08	0.05		Na pole
Ba pole	0.00	0.00	0.00	0.00	0.00	0.00	0.00	0.01		Ba pole

fusion of the mineral was achieved by sharply focusing the laser spot on the grain. The mass spectrometer is a VG[®] 3600 working with a Daly[®] detector. Static measurements of argon isotopes correspond to eleven peak hopping scans. Backgrounds of the extraction and purification line were measured every first or third step and subtracted from each argon isotope from the subsequent gas fractions. Typical blank values were in the ranges $5.6 \times 10^{-13} < M/e40 < 14.0 \times 10^{-13}$, $0.05 \times 10^{-13} < M/e39 < 3.6 \times 10^{-13}$, $0.4 \times 10^{-13} < M/e37 < 1.0 \times 10^{-13}$ and $0.9 \times 10^{-14} < M/e36 < 2.5 \times 10^{-13}$ cm³ STP. All isotopic measurements were corrected for potassium and calcium isotopic interferences, mass discrimination, and atmospheric argon contamination. All errors are quoted at the 1 σ level and do not include the error on the $^{40}\text{Ar}^*/^{39}\text{Ar}_K$ ratio and age of the monitor. The error on the $^{40}\text{Ar}^*/^{39}\text{Ar}_K$ ratio of the monitor is included in the calculation of the plateau age error. To define a plateau age, we need at least three consecutive steps, corresponding to a minimum of 70% of the total ^{39}Ar released, and the individual fraction ages must agree within 2 σ error bars with the integrated age of the plateau segment.

5. $^{40}\text{Ar}/^{39}\text{Ar}$ RESULTS

Twelve experiments were performed on submillimetric fragments from the cortices or the most inner parts (named here-

after nuclei or whole ore) of the concretions. Six and four samples were extracted from the cortices of samples Col4 and Col5, respectively. The positions of the samples are displayed on Figs. 7 and 8. All of the data concerning the age spectra are presented in Table 4. All samples issued from the two cortices (with the exception of sample Col5-a) yield similar age spectra characterized by pronounced increasing staircase shapes in the first 20% of the total $^{39}\text{Ar}_K$ released followed by rather flat segments in intermediate to high temperature steps. These flat segments can show slight irregularities (e.g., Col5-g) or minor increases of the apparent ages from intermediate to high temperature steps (e.g., Col4-c). After the first steps, sample Col5-a shows a decreasing staircase shape in the low temperature steps followed by a rather flat segment.

Sample pairs Col4-c and Col4-e, which were irradiated for very different periods (5 and 70 h), yield remarkably reproducible age spectra (Fig. 7), even in minute details. Six plateau ages are displayed by five samples from the two cortices whereas pseudo-plateau ages ($44.3\% < \text{total } ^{39}\text{Ar}_K \text{ released} < 70\%$) are obtained from all other samples from the two cortices.

The two age spectra from the two nucleus samples (Col4-h and Col5-h) show pronounced bump shapes. Nevertheless, the

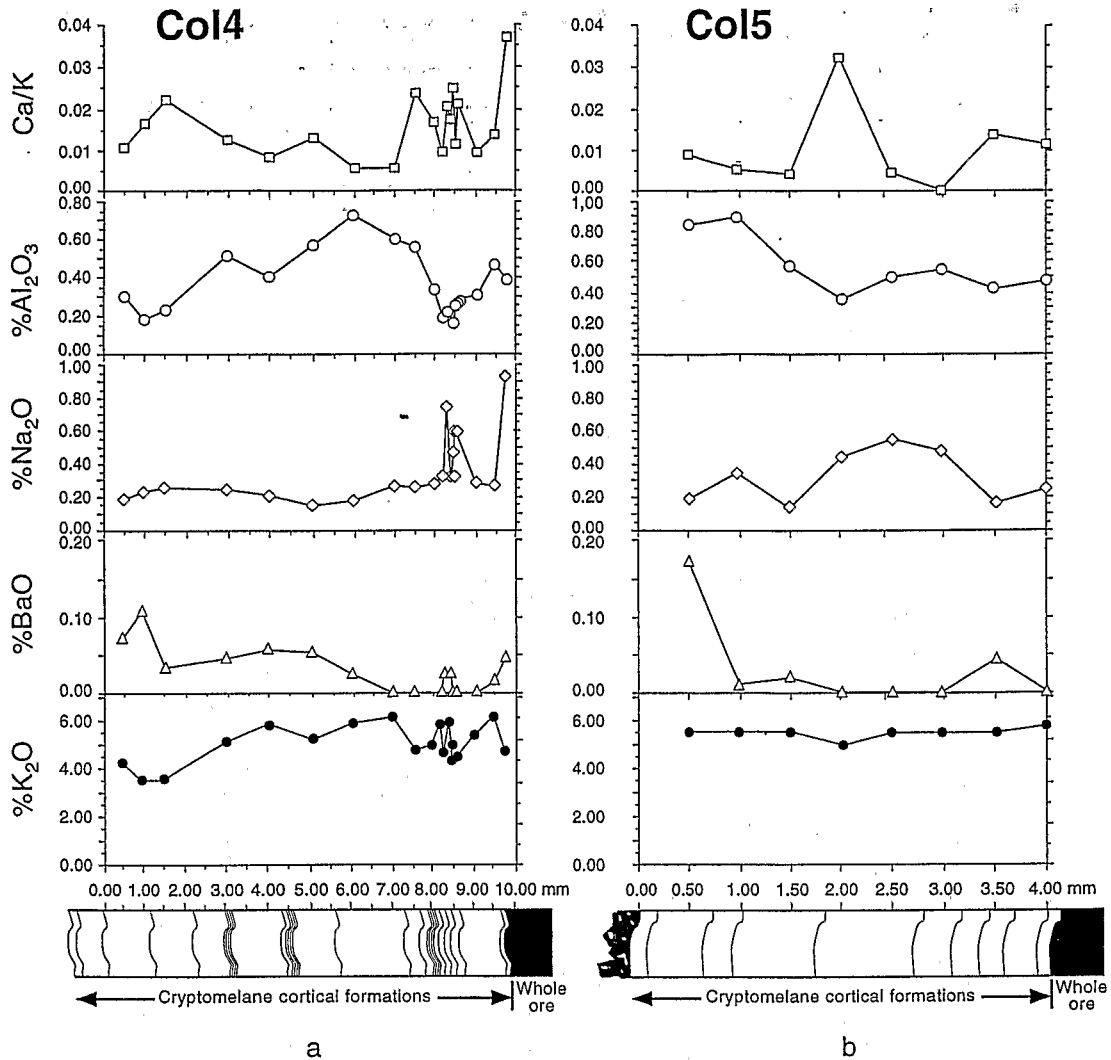


Fig. 6. Electron microprobe transects along the two cortical formations. (a) Evolution of the cations proportions along sample Col 4 cortex. (b) Evolution of the cations proportions along sample Col 5 cortex.

age spectrum of sample Col5-h may define a pseudo-plateau age at 46.6 ± 0.3 Ma (63.8 % of the total $^{39}\text{Ar}_K$ released). The maximum age reached by Col4-h age spectrum is higher, at 53.0 ± 0.9 Ma.

6. DISCUSSION

One of the striking features of the $^{40}\text{Ar}/^{39}\text{Ar}$ results is the systematic staircase shape of the age spectra displayed by most samples from the two cortices. This shape evokes a partial loss of radiogenic argon, provoked either by a thermal event or by an increase of temperature during irradiation. The first possibility seems extremely unlikely in a clearly identified supergene context. Two distinct durations (5 and 70 h) were used for irradiations of each member of two couples of samples (Col4-c and Col4-e). In both cases, the age spectra are perfectly reproducible. This clearly indicates that the age spectrum shape does not result from a partial degassing of radiogenic argon during irradiation.

Within the context of $^{39}\text{Ar}_K$ recoil studies, some authors have obtained age spectra showing increasing staircase shapes from experiments performed on cryptocrystalline materials (e.g., glauconites: Hess and Lippolt, 1986; Smith et al., 1993). The main differences between monophased (or nearly monophased) samples of cryptomelane and glauconite relate to (1) the compactness of the materials, which seems very high for the cryptomelane samples from the two cortices Col4 and Col5, and (2) the size of the constituent crystallites, ≤ 100 nm thick for glauconite (e.g., 5–10 nm according to the study of Smith et al., 1993) to around $1 \mu\text{m}$ thick for cryptomelane needles (e.g., Vasconcelos et al., 1994; Ruffet et al., 1996). Turner and Cadogan (1974) proposed a recoil distance of $0.08 \mu\text{m}$ on average for ^{39}Ar in silicate minerals. This recoil distance, proportional to the recoil energy (0 to 400 keV), is strongly dependent upon the density of the irradiated material. The high density of cryptomelane ($d = 4.3$), the high compactness of the monomineral (or nearly monomineral) aggregates which form

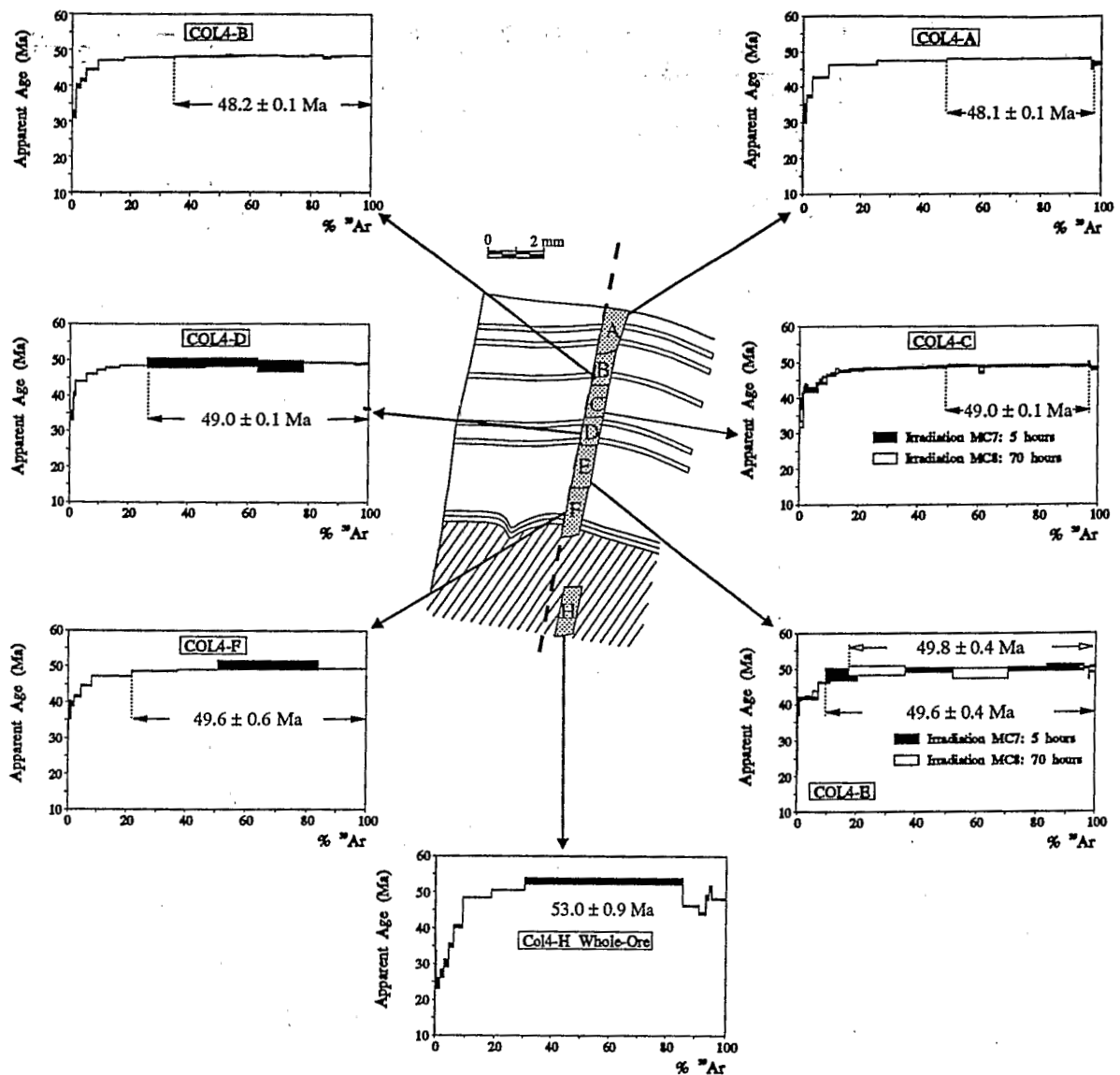


Fig. 7. $^{40}\text{Ar}/^{39}\text{Ar}$ age spectra displayed by the submillimetric fragments extracted from sample Col4. The age error bars for each temperature steps are at the 1σ level. The errors in the J-values are not included.

the successive layers within the cortices of the concretions, and the thickness of the cryptomelane needles are not favorable for significant development of $^{39}\text{Ar}_K$ recoil.

Usually $^{39}\text{Ar}_K$ recoil phenomenon produces age spectra characterized by high apparent ages in the early stages of gas release which decrease during intermediate or high temperature steps (Turner and Cadogan, 1974). Such spectral shapes were also obtained by Ruffet et al. (1996) on manganese oxide samples that were not monomineral. The age spectrum shape of sample Col5-a, which presents some similarities with this classical recoil shape, may be attributed to the presence of impurities such as iron oxides or clay minerals, as observed by optical microscopy and electron microprobe on the outermost face of the cortex.

The staircase shape in the low to intermediate temperature steps of samples from the two cortices could be related to the presence of a younger cryptomelane generation not detected

during petrographical study of the analyzed samples. This is illustrated by two samples from the cortex of concretion Col4. The two age spectra displayed by samples Col4-c and Col4-e show concordant apparent ages in the first 5% of $^{39}\text{Ar}_K$ released, which define small pseudo-plateau ages at 42.9 ± 0.2 Ma (4.2% of $^{39}\text{Ar}_K$ released, 6 steps) and 42.1 ± 0.1 Ma (4.3% of $^{39}\text{Ar}_K$ released, 3 steps), respectively. The correlation diagram technique ($^{36}\text{Ar}/^{40}\text{Ar}$ vs. $^{39}\text{Ar}/^{40}\text{Ar}$) (Turner, 1971; Roddick et al., 1980; Hanes et al., 1985) allows definition of two isochron ages at 43.3 ± 0.3 Ma (MSWD = 1.3; Col4-c) and 42.2 ± 0.6 Ma (MSWD = 6.6; Col4-e) with $(^{40}\text{Ar}/^{36}\text{Ar})_i$ ratios lower than atmospheric ratio (295.5), at $255.8 \pm 1.4\%$ and $286.3 \pm 0.4\%$. These low $(^{40}\text{Ar}/^{36}\text{Ar})_i$ ratios and the rather high MSWD parameters, although yet frequently observed during isochron analyses of samples from cortices Col4 and Col5, suggest that these ages could be artifacts linked to the presence of secondary alteration phases.

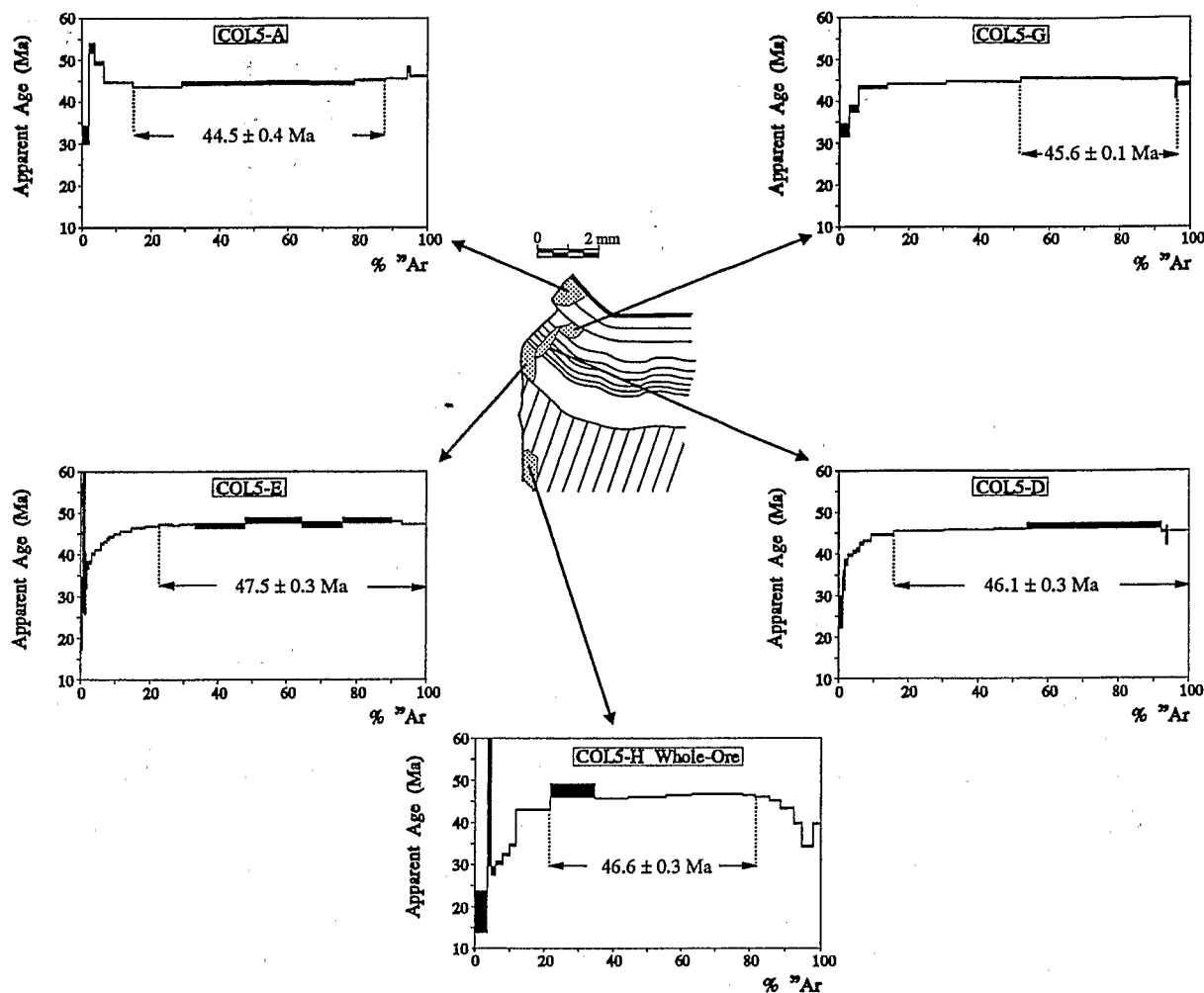


Fig. 8. $^{40}\text{Ar}/^{39}\text{Ar}$ age spectra displayed by the sub-millimetric fragments extracted from sample Col5. Same observation as for Fig. 8.

Another striking feature of the obtained $^{39}\text{Ar}/^{40}\text{Ar}$ results is the steady decrease of the ages (plateau and pseudo-plateau ages, integrated ages and maximum ages of the high temperature steps) from the inner to the outer part of the two cortices as shown on Fig. 9. The electron microprobe profiles performed on the two cortices do not show any regular evolution of the K, Ca, Ba, Al, and Na contents (Fig. 6a and 6b). So, the observed age distributions cannot be linked to any chemical evolution.

On the other hand, Figs. 7 and 8 clearly illustrate the distinct behavior of the samples containing material from the nuclei (Col4-f and -h and Col5-h), probably as a result of their complex mineralogical compositions, which are unlike samples from the two cortices.

For each sample from the cortices, the ratio between the integrated age and the Plateau age obtained remains constant (Fig. 9) whatever its sampling position, especially in sample Col4. This invariability suggests that the two observed age trends do not result from a progressive destabilization, by any process, from inner to outer part of initially homogeneous systems. These age trends probably express a geological reality, as otherwise shown by the mineralogical and petrographical

studies. The different methods used to investigate the mineralogy suggest that each layer of the cortices is a mineralogical system distinct from the surrounding ones. The steadiness of the two age trends is certainly the best evidence of validity of the obtained ages. Therefore, it is likely that these age gradients reflect the growth of the successive cryptomelane generations in the cortices. In the topic of regular crystalline growth, the $^{40}\text{Ar}/^{39}\text{Ar}$ results allow estimation of average precipitation, or growth, rates of c.a. 1 and 5 mm/Ma for concretions Col5 and Col4, respectively. These rates are within the same order of magnitude as those proposed by Vasconcelos et al. (1994).

Within cortex of sample Col4, plateau or pseudo-plateau ages range from 48.1 ± 0.1 Ma to 49.8 ± 0.4 Ma. On the other hand, ages obtained from cortex of sample Col5 range from 44.5 ± 0.4 Ma to 47.5 ± 0.3 Ma. These results show that (1) the ages displayed by the two cortices are inversely correlated to the sampling elevations, and (2) the two age intervals do not overlap.

The two age intervals define a period between 44.5 Ma and 50 Ma during which active weathering was occurring at Tambao. However, They do not allow constraint of the beginning or

Table 4. $^{40}\text{Ar}/^{39}\text{Ar}$ analytical data; 4a: Col 4 samples; 4b: Col 5 samples

V482					
Step n°	#Col 4-a $^{40}\text{Ar}_{\text{atm}}(\%)$	mc8 $^{39}\text{Ar}_{\text{K}}(\%)$	$^{37}\text{Ar}_{\text{Ca}}/^{39}\text{Ar}_{\text{K}}$	$^{40}\text{Ar}^*/^{39}\text{Ar}_{\text{K}}$	J = $1.64471 \cdot 10^{-2}$ Age (Ma)
1	93.2	1.21	0.0480	1.11	32.6 ± 2.8
2	42.0	1.97	0.0330	1.28	37.5 ± 0.4
3	9.7	5.61	0.0150	1.46	42.7 ± 0.2
4	2.1	16.18	0.0040	1.58	46.3 ± 0.1
5	0.8	23.10	0.0060	1.62	47.4 ± 0.1
6	0.4	24.01	0.0060	1.64	48.0 ± 0.1
7	0.3	19.32	0.0060	1.65	48.2 ± 0.1
8	0.4	5.06	0.0080	1.65	48.2 ± 0.2
9	3.5	1.03	0.0500	1.58	46.4 ± 1.3
fuse	2.9	2.50	0.0110	1.60	46.9 ± 0.5

V504					
Step n°	#Col 4-b $^{40}\text{Ar}_{\text{atm}}(\%)$	mc8 $^{39}\text{Ar}_{\text{K}}(\%)$	$^{37}\text{Ar}_{\text{Ca}}/^{39}\text{Ar}_{\text{K}}$	$^{40}\text{Ar}^*/^{39}\text{Ar}_{\text{K}}$	J = $1.64358 \cdot 10^{-2}$ Age (Ma)
1	118.3	0.01	1.8630	-	-
2	78.6	1.43	0.0360	1.09	32.0 ± 1.0
3	38.8	1.43	0.0360	1.35	39.7 ± 0.6
4	20.9	1.95	0.0100	1.42	41.5 ± 0.4
5	8.6	4.00	-	1.52	44.5 ± 0.2
6	2.8	8.75	0.0050	1.61	47.0 ± 0.1
7	1.1	8.46	0.0010	1.63	47.8 ± 0.1
8	0.9	8.49	0.0370	1.64	47.9 ± 0.1
9	0.8	6.30	0.0010	1.64	48.0 ± 0.1
10	0.6	8.12	0.0020	1.65	48.1 ± 0.1
11	0.7	2.95	0.0050	1.65	48.2 ± 0.2
12	0.4	2.11	-	1.65	48.3 ± 0.3
13	0.7	3.56	0.0070	1.65	48.2 ± 0.2
14	0.4	12.19	0.0070	1.65	48.3 ± 0.1
15	0.7	9.65	0.0060	1.65	48.2 ± 0.1
16	0.2	4.47	0.0100	1.66	48.4 ± 0.121
17	1.3	2.46	0.0080	1.64	47.8 ± 0.3
18	0.8	3.47	0.0080	1.65	48.2 ± 0.2
fuse	0.8	10.20	0.0060	1.65	48.3 ± 0.1

v320					
Step n°	#Col 4-c $^{40}\text{Ar}_{\text{atm}}(\%)$	mc7 $^{39}\text{Ar}_{\text{K}}(\%)$	$^{37}\text{Ar}_{\text{Ca}}/^{39}\text{Ar}_{\text{K}}$	$^{40}\text{Ar}^*/^{39}\text{Ar}_{\text{K}}$	J = $1.16596 \cdot 10^{-3}$ Age (Ma)
1	-	0.00	0.2680	-	-
2	100.0	-	0.0026	-	-
3	57.1	0.00	0.6870	24.51	50.8 ± 168.2
4	71.8	0.02	-	15.40	32.1 ± 13.0
5	74.4	0.06	0.0157	12.85	26.9 ± 5.4
6	72.4	0.21	-	14.44	30.1 ± 1.5
7	67.4	0.22	0.0169	16.36	34.1 ± 1.4
8	58.1	0.26	0.0097	18.45	38.4 ± 1.7
9	42.9	0.34	0.0066	19.47	40.5 ± 1.0
10	28.7	0.31	0.0180	19.68	40.9 ± 1.0
11	15.0	0.47	0.0097	20.66	42.9 ± 0.6
12	9.3	0.39	0.0143	20.73	43.1 ± 1.1
13	6.1	0.61	0.0017	20.84	43.3 ± 0.5
14	5.1	0.74	0.0024	20.40	42.4 ± 0.5
15	4.0	0.97	0.0040	20.61	42.8 ± 0.3
16	4.2	0.99	0.0084	20.63	42.9 ± 0.3
17	2.5	1.02	0.0075	21.22	44.1 ± 0.4
18	2.5	1.13	0.0076	21.64	45.0 ± 0.4
19	1.4	1.24	0.0033	22.13	46.0 ± 0.3
20	1.4	1.63	0.0035	22.40	46.5 ± 0.2
21	0.8	1.59	0.0048	22.64	47.0 ± 0.2
22	0.2	2.02	0.0055	22.81	47.3 ± 0.2
23	0.5	3.17	0.0051	22.81	47.4 ± 0.1
24	0.6	4.32	0.0053	22.91	47.6 ± 0.1
25	0.4	6.20	0.0057	23.14	48.0 ± 0.1

the end of the history of this weathering sequence. This observed age interval (44.5 up to 50 Ma) is nevertheless concordant with the age interval defined for the weathering sequence

of Azul in Brazil (Vasconcelos et al., 1994; Ruffet et al., 1996), suggesting widespread occurrence of such weathering processes during this period. However, it is not possible to link this

Table 4a (continued)

Step n°	$^{40}\text{Ar}_{\text{atm.}}$ (%)	$^{39}\text{Ar}_K$ (%)	$^{37}\text{Ar}_{\text{Ca}}/^{39}\text{Ar}_K$	$^{40}\text{Ar}^*/^{39}\text{Ar}_K$	Age (Ma)
26	0.3	7.22	0.0060	23.19	48.1 ± 0.1
27	0.3	7.80	0.0055	23.26	48.3 ± 0.1
28	0.2	6.55	0.0050	23.35	48.5 ± 0.1
29	0.2	5.66	0.0056	23.47	48.7 ± 0.1
30	0.1	5.32	0.0049	23.58	48.8 ± 0.1
31	0.7	1.60	0.0035	22.67	47.1 ± 0.2
32	0.2	8.70	0.0057	23.48	48.7 ± 0.1
33	0.2	6.95	0.0053	23.50	48.8 ± 0.1
34	0.2	5.81	0.0051	23.44	48.7 ± 0.1
35	0.0	7.41	0.0040	23.54	48.8 ± 0.1
36	0.2	4.92	0.0027	23.47	48.7 ± 0.1
37	0.5	1.62	0.0006	23.58	48.9 ± 0.2
fuse	1.8	2.50	0.0060	23.01	47.8 ± 0.2

V484					
Step n°	#Col 4-c	mc8	J = 1.64241 · 10 ⁻²		
Step n°	$^{40}\text{Ar}_{\text{atm.}}$ (%)	$^{39}\text{Ar}_K$ (%)	$^{37}\text{Ar}_{\text{Ca}}/^{39}\text{Ar}_K$	$^{40}\text{Ar}^*/^{39}\text{Ar}_K$	Age (Ma)
1	75.6	0.02	0.2080	1.72	50.1 ± 22.6
2	79.2	1.35	0.0180	1.11	32.7 ± 0.9
3	29.9	4.77	0.0090	1.43	41.9 ± 0.3
4	9.7	3.10	0.0150	1.51	44.2 ± 0.2
5	5.7	3.07	0.0110	1.59	46.4 ± 0.3
6	4.2	0.99	-	1.63	47.6 ± 0.6
7	2.3	3.46	0.0010	1.63	47.6 ± 0.2
8	1.4	4.23	0.0030	1.64	48.0 ± 0.2
9	1.0	12.22	0.0080	1.65	48.3 ± 0.1
10	0.5	9.98	0.0060	1.67	48.7 ± 0.1
11	0.3	6.58	0.0070	1.68	49.0 ± 0.1
12	0.0	3.61	0.0080	1.68	49.2 ± 0.2
13	0.0	3.67	0.0090	1.68	49.2 ± 0.2
14	0.0	3.77	0.0080	1.68	49.2 ± 0.2
15	0.9	2.50	0.0130	1.67	48.8 ± 0.2
16	0.4	5.72	0.0080	1.68	49.0 ± 0.1
17	0.3	27.34	0.0070	1.68	49.1 ± 0.1
18	0.2	0.66	0.0050	1.68	49.2 ± 0.1
fuse	0.8	2.96	0.0090	1.66	48.4 ± 0.1

V505					
Step n°	#Col 4-d	mc8	J = 1.64132 · 10 ⁻²		
Step n°	$^{40}\text{Ar}_{\text{atm.}}$ (%)	$^{39}\text{Ar}_K$ (%)	$^{37}\text{Ar}_{\text{Ca}}/^{39}\text{Ar}_K$	$^{40}\text{Ar}^*/^{39}\text{Ar}_K$	Age (Ma)
1	100.2	0.00	1.5000	-	-
2	86.6	1.30	0.0130	1.17	34.3 ± 1.4
3	35.5	0.73	0.0170	1.38	40.3 ± 0.5
4	12.5	3.72	0.0350	1.51	44.0 ± 0.2
5	5.8	3.57	0.0160	1.58	46.1 ± 0.2
6	3.7	2.84	0.0120	1.62	47.2 ± 0.1
7	2.0	4.68	0.0100	1.64	47.9 ± 0.1
8	1.1	9.32	0.0060	1.66	48.3 ± 0.1
9	0.0	19.57	-	1.68	49.1 ± 1.5
10	0.0	17.23	-	1.69	49.3 ± 1.3
11	2.3	14.94	-	1.65	48.2 ± 1.6
12	0.4	8.81	0.0060	1.69	49.3 ± 0.1
13	0.5	4.75	0.0090	1.69	49.3 ± 0.1
14	0.6	3.47	0.0030	1.68	49.2 ± 0.1
15	1.1	1.45	0.0050	1.67	48.9 ± 0.3
16	1.3	1.27	0.0150	1.67	48.9 ± 0.3
fuse	2.2	2.35	0.0070	1.68	49.0 ± 0.2

v328					
Step n°	#Col 4-e	mc7	J = 1.16314 · 10 ⁻³		
Step n°	$^{40}\text{Ar}_{\text{atm.}}$ (%)	$^{39}\text{Ar}_K$ (%)	$^{37}\text{Ar}_{\text{Ca}}/^{39}\text{Ar}_K$	$^{40}\text{Ar}^*/^{39}\text{Ar}_K$	Age (Ma)
1	58.7	0.01	0.1810	32.15	66.2 ± 47.3
2	76.8	0.29	0.0114	16.51	34.3 ± 1.4
3	74.1	0.52	0.0104	18.24	37.9 ± 0.9

results to a vertical age gradient, with respect to weathering path, as done by Vasconcelos et al. (1992), because of our limited number of samples.

Geomorphological studies of West African indurated reliefs

suggested that the highest ones, the Bauxitic surface and the adjacent Fe-Mn crust, may have developed respectively from the Eocene to the Pliocene (Boulet, 1970; Grandin, 1976; Michel, 1978). On the basis of petrological studies, Boulangé

Table 4a (continued)

Step n°	$^{40}\text{Ar}_{\text{atm.}}(\%)$	$^{39}\text{Ar}_{\text{K}}(\%)$	$^{37}\text{Ar}_{\text{Ca}}/^{39}\text{Ar}_{\text{K}}$	$^{40}\text{Ar}^*/^{39}\text{Ar}_{\text{K}}$	Age (Ma)
4	51.9	0.78	0.0037	20.08	41.7 ± 0.5
5	22.3	0.98	0.0149	20.10	41.7 ± 0.2
6	9.4	2.56	0.0081	20.44	42.4 ± 0.1
7	5.6	1.77	0.0078	21.14	43.8 ± 0.2
8	2.3	2.51	0.0073	22.34	46.3 ± 0.1
9	-	11.00	0.0016	23.43	48.5 ± 1.8
10	0.1	32.79	0.0070	23.91	49.5 ± 0.5
11	0.9	29.92	0.0104	24.08	49.8 ± 0.4
12	-	12.81	0.0168	24.33	50.3 ± 1.0
13	0.5	1.66	0.0091	24.25	50.2 ± 0.2
14	3.8	0.28	0.0187	23.25	48.1 ± 1.0
fuse	3.0	2.14	0.0110	23.70	49.1 ± 0.2

V483		#Col 4-e	mc8	J = 1.64022 · 10 ⁻²		
Step n°	$^{40}\text{Ar}_{\text{atm.}}(\%)$	$^{39}\text{Ar}_{\text{K}}(\%)$	$^{37}\text{Ar}_{\text{Ca}}/^{39}\text{Ar}_{\text{K}}$	$^{40}\text{Ar}^*/^{39}\text{Ar}_{\text{K}}$	Age (Ma)	
1	91.6	0.05	0.0330	0.92	27.1 ± 6.0	
2	46.6	6.85	0.0070	1.43	41.8 ± 0.3	
3	6.5	4.12	0.0070	1.58	46.2 ± 0.1	
4	2.8	6.52	0.0080	1.65	48.2 ± 0.1	
5	1.2	18.88	0.0180	1.70	49.5 ± 1.2	
6	0.7	15.77	0.0070	1.72	50.2 ± 0.1	
7	3.7	18.45	0.0070	1.67	48.7 ± 1.5	
8	0.3	12.75	0.0070	1.73	50.5 ± 0.1	
9	0.1	6.97	0.0060	1.73	50.5 ± 0.1	
10	0.5	4.05	0.0090	1.73	50.43 ± 0.1	
11	0.5	1.71	0.0130	1.73	50.3 ± 0.3	
12	1.2	1.96	0.0090	1.72	50.3 ± 0.2	
fuse	0.3	1.91	0.0050	1.73	50.5 ± 0.2	

v322		#Col 4-f	mc7	J = 1.16173 · 10 ⁻³		
Step n°	$^{40}\text{Ar}_{\text{atm.}}(\%)$	$^{39}\text{Ar}_{\text{K}}(\%)$	$^{37}\text{Ar}_{\text{Ca}}/^{39}\text{Ar}_{\text{K}}$	$^{40}\text{Ar}^*/^{39}\text{Ar}_{\text{K}}$	Age (Ma)	
1	92.9	0.22	-	16.04	33.3 ± 4.1	
2	92.4	0.95	0.0056	18.24	37.8 ± 2.7	
3	45.5	1.02	0.0061	19.06	39.5 ± 0.6	
4	18.1	2.40	0.0083	20.10	41.7 ± 0.3	
5	6.8	3.58	0.0050	21.52	44.6 ± 0.2	
6	2.4	13.46	0.0073	22.85	47.3 ± 0.1	
7	1.1	15.35	0.0079	23.51	48.6 ± 0.1	
8	1.1	13.68	0.0082	23.74	49.1 ± 0.1	
9	-	33.18	-	24.32	50.3 ± 1.3	
fuse	1.3	16.16	0.0078	23.91	49.4 ± 0.1	

v324		#Col 4-h	mc7	J = 1.16019 · 10 ⁻³		
Step n°	$^{40}\text{Ar}_{\text{atm.}}(\%)$	$^{39}\text{Ar}_{\text{K}}(\%)$	$^{37}\text{Ar}_{\text{Ca}}/^{39}\text{Ar}_{\text{K}}$	$^{40}\text{Ar}^*/^{39}\text{Ar}_{\text{K}}$	Age (Ma)	
1	91.1	0.01	0.4020	50.64	103.0 ± 100.4	
2	95.6	0.51	0.0275	14.11	29.3 ± 4.3	
3	90.6	1.28	0.0191	11.84	24.6 ± 1.6	
4	80.5	1.25	0.0214	13.10	27.2 ± 1.3	
5	74.6	1.44	0.0221	14.52	30.1 ± 1.1	
6	62.1	1.74	0.0305	16.96	35.2 ± 0.7	
7	50.9	3.05	0.0333	19.53	40.4 ± 0.5	
8	26.0	9.68	0.0165	23.45	48.4 ± 0.2	
9	12.5	11.52	0.0113	24.43	50.4 ± 0.1	
10	3.5	55.27	0.0030	25.72	53.0 ± 0.9	
11	13.3	5.42	0.0272	22.38	46.2 ± 0.2	
12	15.5	2.27	0.0319	21.38	44.2 ± 0.4	
13	11.4	1.09	0.0132	23.54	48.6 ± 0.7	
14	8.2	0.91	0.0048	24.76	51.1 ± 0.9	
fuse	11.8	4.57	0.0135	23.35	48.2 ± 0.2	

(1984) suggested that a genetic relationship may exist between the bauxitic surface and the adjacent Fe-Mn pisolitic crust. This author thinks that Fe (or Mn), that resulted from leaching of the parent rock during the formation of the bauxitic surface precipitated nearby to form the Fe or Mn pisolitic crust. These in

situ (at the landscape scale) weathering activities could have been effective during the Eocene to Miocene period, in the presence of favorable (humid equatorial rainforest) climatic conditions. Our ages, ranging from 44.5 Ma to 50 Ma, obtained for samples from such a transitional lateritic system clearly

Table 4b

V479 #Col 5-a mc8 J= 1.63447 . 10 ⁻²					
Step n°	⁴⁰ Ar _{atm.} (%)	³⁹ Ar _K (%)	³⁷ Ar _{Ca} / ³⁹ Ar _K	⁴⁰ Ar*/ ³⁹ Ar _K	Age (Ma)
1	92.3	2.16	0.0114	1.1	32.1 ± 2.3
2	76.4	1.63	0.00840	1.8	53.0 ± 1.2
3	43.4	2.66	0.0097	1.7	49.3 ± 0.4
4	17.7	8.30	0.0079	1.5	44.8 ± 0.2
5	13.8	14.23	0.0062	1.5	43.6 ± 0.1
6	5.8	49.90	0.0016	1.5	44.6 ± 0.5
7	2.6	9.10	0.0080	1.5	45.2 ± 0.1
8	1.7	6.27	0.0063	1.6	45.5 ± 0.1
9	2.4	0.79	0.0027	1.6	47.8 ± 0.6
fuse	2.6	4.96	0.0096	1.6	46.2 ± 0.1

V468 #Col 5-g mc8 J= 1.62183 . 10 ⁻²					
Step n°	⁴⁰ Ar _{atm.} (%)	³⁹ Ar _K (%)	³⁷ Ar _{Ca} / ³⁹ Ar _K	⁴⁰ Ar*/ ³⁹ Ar _K	Age (Ma)
1	83.00	3.04	0.0450	1.1	33.0 ± 1.6
2	32.1	2.51	0.0420	1.3	38.3 ± 0.9
3	8.3	8.29	0.0140	1.5	43.4 ± 0.3
4	6.5	16.77	0.0110	1.5	44.2 ± 0.2
5	3.2	21.32	0.0090	1.5	44.7 ± 0.1
6	1.3	28.26	0.0080	1.6	45.6 ± 0.1
7	1.3	15.41	0.0110	1.6	45.4 ± 0.2
8	7.1	0.67	0.0230	1.5	42.9 ± 2.3
fuse	3.3	3.75	0.0040	1.5	44.1 ± 0.5

V506 #Col 5-d mc8 J= 1.62811 . 10 ⁻²					
Step n°	⁴⁰ Ar _{atm.} (%)	³⁹ Ar _K (%)	³⁷ Ar _{Ca} / ³⁹ Ar _K	⁴⁰ Ar*/ ³⁹ Ar _K	Age (Ma)
1	98.6	0.18	0.0030	0.46	13.5 ± 8.3
2	96.3	1.00	-	0.89	26.1 ± 3.8
3	90.0	0.16	-	1.03	29.9 ± 5.0
4	84.8	0.43	-	1.16	33.6 ± 2.4
5	66.9	0.97	-	1.31	38.0 ± 0.8
6	29.2	1.37	-	1.37	39.7 ± 0.3
7	18.4	1.14	0.0080	1.39	40.5 ± 0.4
8	12.8	0.82	0.0240	1.41	41.0 ± 0.5
9	7.9	1.24	0.0080	1.46	42.4 ± 0.3
10	7.8	2.07	0.0200	1.49	43.1 ± 0.2
11	6.1	6.53	0.0160	1.54	44.6 ± 0.1
12	2.2	14.33	0.0050	1.57	45.4 ± 0.1
13	1.0	14.27	0.0100	1.58	45.8 ± 0.1
14	0.7	9.41	0.0060	1.58	45.9 ± 0.1
15	0.0	38.15	-	1.61	46.6 ± 0.6
16	2.0	1.50	0.0170	1.56	45.2 ± 0.3
17	3.5	0.25	0.0370	1.52	44.1 ± 2.2
fuse	2.0	6.18	0.0100	1.56	45.4 ± 0.1

V485 #Col 5-e mc8 J= 1.62603 . 10 ⁻²					
Step n°	⁴⁰ Ar _{atm.} (%)	³⁹ Ar _K (%)	³⁷ Ar _{Ca} / ³⁹ Ar _K	⁴⁰ Ar*/ ³⁹ Ar _K	Age (Ma)
1	22.5	0.00	0.0110	266.16	3018.1 ± 2013.6
2	98.0	0.02	0.0460	0.42	12.2 ± 11.5
3	97.5	0.16	0.0210	0.81	23.5 ± 6.2
4	97.7	0.09	0.0590	0.95	27.7 ± 7.0
5	98.3	0.24	0.0330	0.89	26.0 ± 8.5
6	95.5	0.23	-	3.72	106.0 ± 34.6
7	98.2	0.42	-	1.80	52.1 ± 25.3
8	97.4	0.38	0.0060	1.14	33.1 ± 7.4
9	93.4	0.43	0.0100	1.21	35.0 ± 3.0
10	74.3	0.48	0.0170	1.30	37.6 ± 0.9
11	51.1	0.69	0.0090	1.32	38.3 ± 0.5
12	34.2	0.21	0.0090	1.37	39.7 ± 1.0
13	27.0	0.92	0.0070	1.38	40.1 ± 0.2
14	16.4	1.59	0.0160	1.42	41.2 ± 0.1

Table 4b (continued)

Step n°	$^{40}\text{Ar}_{\text{atm}}$ (%)	$^{39}\text{Ar}_{\text{K}}$ (%)	$^{37}\text{Ar}_{\text{Ca}}/^{39}\text{Ar}_{\text{K}}$	$^{40}\text{Ar}^*/^{39}\text{Ar}_{\text{K}}$	Age (Ma)
15	9.8	0.96	0.0120	1.47	42.6 ± 0.2
16	7.9	0.78	0.0230	1.49	43.0 ± 0.3
17	6.4	0.68	0.0200	1.51	43.7 ± 0.3
18	5.4	1.24	0.0130	1.53	44.3 ± 0.2
19	4.4	1.93	0.0090	1.55	45.0 ± 0.1
20	3.8	3.23	0.0060	1.58	45.6 ± 0.1
21	2.4	3.92	0.0060	1.60	46.3 ± 0.1
22	1.7	4.02	0.0080	1.62	46.8 ± 0.1
23	1.3	4.06	0.0070	1.63	47.2 ± 0.2
24	1.5	2.06	0.0080	1.62	47.0 ± 0.1
25	1.1	4.59	0.0060	1.63	47.3 ± 0.1
25	2.3	14.41	0.0160	1.62	46.8 ± 0.7
27	-	16.52	-	1.66	48.1 ± 0.8
28	2.3	11.64	0.0040	1.63	47.1 ± 0.8
29	-	14.20	0.0090	1.67	48.2 ± 0.7
30	0.6	3.04	0.0060	1.66	48.0 ± 0.1
fuse	1.4	6.86	0.0060	1.63	47.2 ± 0.1

V503 Step n°	#Col 5-h $^{40}\text{Ar}_{\text{atm}}$ (%)	mc8 $^{39}\text{Ar}_{\text{K}}$ (%)	$^{37}\text{Ar}_{\text{Ca}}/^{39}\text{Ar}_{\text{K}}$	$^{40}\text{Ar}^*/^{39}\text{Ar}_{\text{K}}$	J= 1.61973 · 10 ⁻² Age (Ma)
1	97.4	3.58	0.4100	0.65	18.8 ± 5.0
2	92.3	1.06	0.2960	1.59	45.9 ± 16.2
3	86.3	1.30	0.4530	0.98	28.5 ± 1.1
4	67.2	1.95	0.2000	1.05	30.4 ± 0.5
5	48.7	2.09	0.0790	1.12	32.4 ± 0.3
6	36.8	1.84	0.0480	1.20	34.7 ± 0.3
7	17.2	9.90	0.0310	1.49	43.1 ± 0.1
8	3.3	13.13	-	1.65	47.5 ± 1.6
9	5.6	9.50	0.0260	1.59	45.7 ± 0.1
10	4.8	11.04	0.0230	1.60	46.0 ± 0.1
11	4.4	7.73	0.0240	1.61	46.4 ± 0.1
12	4.0	5.54	0.0210	1.62	46.7 ± 0.1
13	4.0	5.00	0.0230	1.62	46.8 ± 0.1
14	4.0	4.17	0.0230	1.62	46.8 ± 0.1
15	4.3	3.63	0.0250	1.61	46.5 ± 0.1
16	4.8	4.03	0.0270	1.60	46.1 ± 0.1
17	5.5	3.19	0.0280	1.57	45.2 ± 0.1
18	7.2	3.76	0.0370	1.50	43.4 ± 0.1
19	11.2	2.18	0.0460	1.38	39.8 ± 0.3
20	16.4	3.09	0.0560	1.18	34.2 ± 0.2
fuse	8.4	2.29	0.0420	1.38	39.7 ± 0.1

support this hypothesis. Further works would allow us to extend our investigations through the whole deposit and then to propose a complete history of these Mn-laterites.

7. CONCLUSION

1. This work improves analytical protocol for $^{40}\text{Ar}/^{39}\text{Ar}$ dating of manganese oxides initiated at the beginning of the decade by Segev et al. (1991), using K-Ar method, and Vasconcelos et al. (1992, 1994), using K-Ar and $^{40}\text{Ar}/^{39}\text{Ar}$ argon-ion laser probe method. We are now able to reduce problems related to phase mixing because of (A) the use of a laser probe, which allows to work on small samples, and also (B) rigorous sampling based on previous precise petrographical studies of the samples. This is necessary for unambiguous interpretation of $^{40}\text{Ar}/^{39}\text{Ar}$ results on such samples.
2. The twelve sets of $^{40}\text{Ar}/^{39}\text{Ar}$ determination yielded twelve plateau and pseudo-plateau ages that show, from the inner to

the outer parts of the two cortices, regular progressions from 48.1 ± 0.1 Ma up to 49.6 ± 0.6 Ma (sample Col4) and from 44.5 ± 0.5 Ma up to 47.5 ± 0.3 Ma (sample Col5). These results suggest precipitation or growth rates in the range of 1–5 mm/Ma.

3. This age interval (44.5 ± 0.5 Ma → 49.6 ± 0.6 Ma) indicates that the weathering profile of Tambao was in the process of functioning during the Eocene. It suggests, taking into consideration the climatic conditions necessary to development of lateritic systems, that this area was under humid tropical conditions at that time.
4. These results are the first reliable ages obtained on cryptomelane from a West African weathering profile. In accordance with the geomorphological study of the area performed by Grandin (1976), they are in agreement with the hypothesis of a genetic relationship between bauxites of the African Surface and the adjacent Fe-Mn pisolitic crust as proposed by Boulangé (1983).

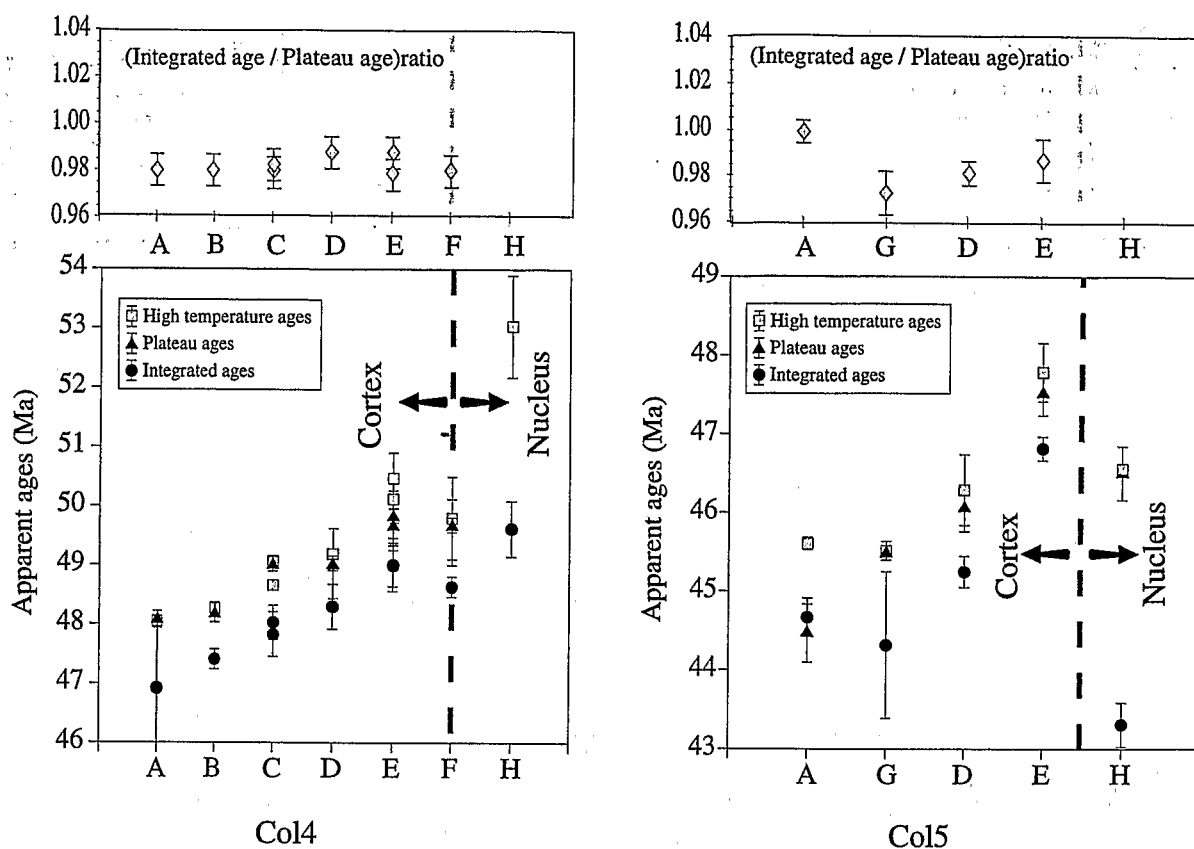


Fig. 9. Evolutions of the Integrated ages, Maximum ages, Plateau ages and of the (Integrated age/Plateau age) ratio along the two cortices. The high ratio value observed for sample Col5a cannot be taken into account because of the saddle shaped age spectrum yielded by this fragment.

Acknowledgements—We specially thank Professor D. Nahon for having helping us in our microscopic study as well as Georges Grandin for fieldwork. E. Brown is thanked for improving the English. This study was financially supported by the grants DBT Fleuves et Erosion and 97Prose 20 of INSU, and by ORSTOM. We also thank the two anonymous reviewers.

REFERENCES

- Beauvais A. and Colin F. (1993) Formation and transformation processes of iron duricrust systems in tropical environment. *Chem. Geol.* **106**, 77–101.
- Boulangé B. (1983) Les formations bauxitiques latéritiques de Côte-d'Ivoire. Les faciès, leur distribution et l'évolution du modèle. *Mém. ORSTOM* **175**, 363 p.
- Boulet R. (1970) La géomorphologie et les principaux types de sol en Haute-Volta septentrionale. *Cah. ORSTOM, ser. Pédol.* **8**, 245–271.
- Brown E. T., Bourlès D. L., Colin F., Sanfo Z., Raisbeck G. M., and Yiou F. (1994) The development of Iron crust lateritic systems in Burkina Faso, West Africa examined with in situ produced cosmogenic nuclides. *Earth Planet. Sci. Lett.* **124**, 19–33.
- Byström A. and Byström A. M. (1950) The crystal structure of Hollandite, the related manganese oxide minerals, and α - MnO_2 . *Acta Cryst.* **3**, 146–154.
- Chukhrov F. V., Shanin L. L., and Yermilov L. P. (1966) Feasibility of absolute-age determination for potassium-carrying manganese minerals. *Int. Geo. Rev.* **8**, 278–280.
- Colin F., Sanfo Z., Brown E. T., Bourlès D., and Edou Minko A. (1997) Gold: A tracer of the dynamics of laterites. *Geology* **25**, 81–84.
- Grandin G. (1976) Aplissements cuirassés et enrichissement des gisements de manganèse dans quelques régions d'Afrique de l'Ouest. *Mém. ORSTOM*, **82**, 275 p.
- Hanes J. A., York D., and Hall C. M. (1985) An $^{40}Ar/^{39}Ar$ geochronological and electron microprobe investigation of an archean pyroxenite and its bearing on ancient atmospheric compositions. *Canadian J. Earth. Sci.* **22**, 947–958.
- Hess J. C. and Lippolt H. J. (1986) Kinetics of argon isotopes during neutron irradiation: ^{39}Ar loss from minerals as a source of error in $^{40}Ar/^{39}Ar$ dating. *Chem. Geol.* **59**, 223–236.
- Holtrop J. F. (1965) The manganese deposits of the Guyana shield. *Econ. Geol.* **60**, 1185–1212.
- McKenzie R. M. (1989) Manganese Oxides and Hydroxides. In *Minerals in Soil Environments* (ed. J. B. Dixon and S. B. Weed), 2nd ed. pp. 439–465. Soil Sci. Soc. Amer.
- Michel P. (1978) Cuirasses bauxitiques et ferrugineuses d'Afrique Occidentale - Aperçu chronologique. *Trav. Doc. Géogr. Trop. CEGET CNRS* **33**, 11–32.
- Nahon D. (1986) Evolution of iron crust in tropical landscapes. In *Rates of Chemical Weathering of Rocks and Minerals* (ed. S. H. Colemans and D. P. Dethier), pp. 169–191. Academic Press.
- Nahon D. (1991) *Introduction to the Petrology of Soils and Chemical Weathering*. Wiley.
- Nahon D., Beauvais A., Nziengui-Mapangou P., and Ducloux J. (1984) Chemical weathering of manganese-garnets under lateritic conditions in northwest Ivory Coast (West Africa). *Chem. Geol.* **45**, 53–71.
- Nahon D., Beauvais A., and Trescases J. J. (1985) Manganese concentration through chemical weathering of metamorphic rocks under lateritic conditions. In *The Chemistry of Weathering* (ed. J. I. Drever), pp. 277–291. Reidel Publ. Co.
- Nahon D., Boulangé B., and Colin F. (1991) Metallogeny of weathering: An introduction. In *Development in Earth Surface Processes 2* (ed. J. P. Martin and W. Chesworth), pp. 445–471. Elsevier.
- Perseil E. A. and Grandin G. (1978) Evolution minéralogique du

- manganèse dans trois gisements d'Afrique de l'Ouest: Mokta, Tambao, Nsuta. *Mineral. Depos.* **13**, 295-311.
- Perseil E. A. and Grandin G. (1985) Altération supergène des protogènes à grenats manganésifères dans quelques gisements d'Afrique de l'Ouest. *Mineral. Depos.* **20**, 211-219.
- Picot P. and Trinquard R. (1969) La manganosite (MnO) du gîte de manganèse de Tambao (Haute-Volta). *Bull. Soc. fr. Minér. Cristallogr.* **92**, 500-502.
- Roddick J. C., Cliff R. A., and Rex D. C. (1980) The evolution of excess argon in alpine biotites-A $^{40}\text{Ar}/^{39}\text{Ar}$ analysis. *Earth Planet. Sci. Lett.* **48**, 185-208.
- Roddick J. C. (1983). High precision intercalibration of $^{40}\text{Ar}/^{39}\text{Ar}$ standards. *Geochim. Cosmochim. Acta* **47**, 887-898.
- Ruffet G., Féraud G., and Amouric M. (1991) Comparison of $^{40}\text{Ar}/^{39}\text{Ar}$ conventional and laser dating of biotites from the North Trégor Batholith *Geochim. Cosmochim. Acta* **55**, 1675-1688.
- Ruffet G. et al. (1996) A geochronological $^{40}\text{Ar}/^{39}\text{Ar}$ and $^{87}\text{Rb}/^{87}\text{Sr}$ study of K-Mn oxides from the weathering sequence of Azul (Brazil). *Geochim. Cosmochim. Acta* **60**, 2219-2232.
- Sanfo Z. (1994) Histoire des champs latéritiques aurifères de la région d'Aribinda (Nord Burkina Faso): Application à la prospection en zone sub-sahélienne. Th. 3ème Cycle, Univ. Aix-Marseille III.
- Segev A., Halicz L., Lang B., and Steinitz G. (1991) K-Ar dating of manganese minerals from the Eisenbach region, Black Forest, Southwest Germany. *Schweiz. Mineral. Petrogr. Mitt.* **71**, 101-114.
- Smith P. E., Evensen N. M., and York D. (1993). First successful $^{40}\text{Ar}/^{39}\text{Ar}$ dating of glauconies: Argon recoil in single grains of cryptocrystalline material. *Geology* **21**, 41-44.
- Turner G. (1971) $^{40-39}\text{Ar}$ ages from the lunar maria. *Earth Planet. Sci. Lett.* **11**, 169-191.
- Turner G. and Cadogan P. H. (1974) Possible effects of ^{39}Ar recoil in $^{40}\text{Ar}/^{39}\text{Ar}$ dating. *Proc. 5th Lunar Conf.* **2**, 1601-1615.
- Turner S. and Buseck P. R. (1979) Manganese oxide tunnel structures and their Intergrowths. *Science* **203**, 456-458.
- Turner S. and Buseck P. R. (1981) Todorokite: A new family of naturally occurring manganese oxides. *Science* **212**, 1024-1027.
- Vasconcelos P. M., Becker T. A., Renne P. R., and Brimhall G. H. (1992) Age and duration of weathering by ^{40}K , ^{40}Ar and $^{40}\text{Ar}/^{39}\text{Ar}$ analysis of potassium-manganese oxides. *Science* **58**, 451-455.
- Vasconcelos P. M., Renne P. R., Brimhall G. H., and Becker T. A. (1994) Direct dating of weathering phenomena by $^{40}\text{Ar}/^{39}\text{Ar}$ and K-Ar analysis of supergene K-Mn oxides. *Geochim. Cosmochim. Acta* **58**, 1635-1665.
- Wadsley A. D. (1953) The crystal structure of Psilomelane ($\text{Ba}_2\text{H}_2\text{O}_2\text{Mn}_5\text{O}_{10}$). *Acta Cryst.* **6**, 433-438.
- Yashvili L. P. and Gukasyan R. Kh. (1974) Use of cryptomelane for potassium-argon dating of manganese ore of the Sevkar-Sargyukh deposit, Armenia. *Dokl. Earth Sci. Sect.* **212**, 49-51.
- Zartman R. E. (1964) A geochronological study of the Love Grove Pluton from the Llano uplift, Texas. *J. Petrol.* **5**, 359-408.